Chapter 6

Interaction of Gallic acid with calf thymus DNA

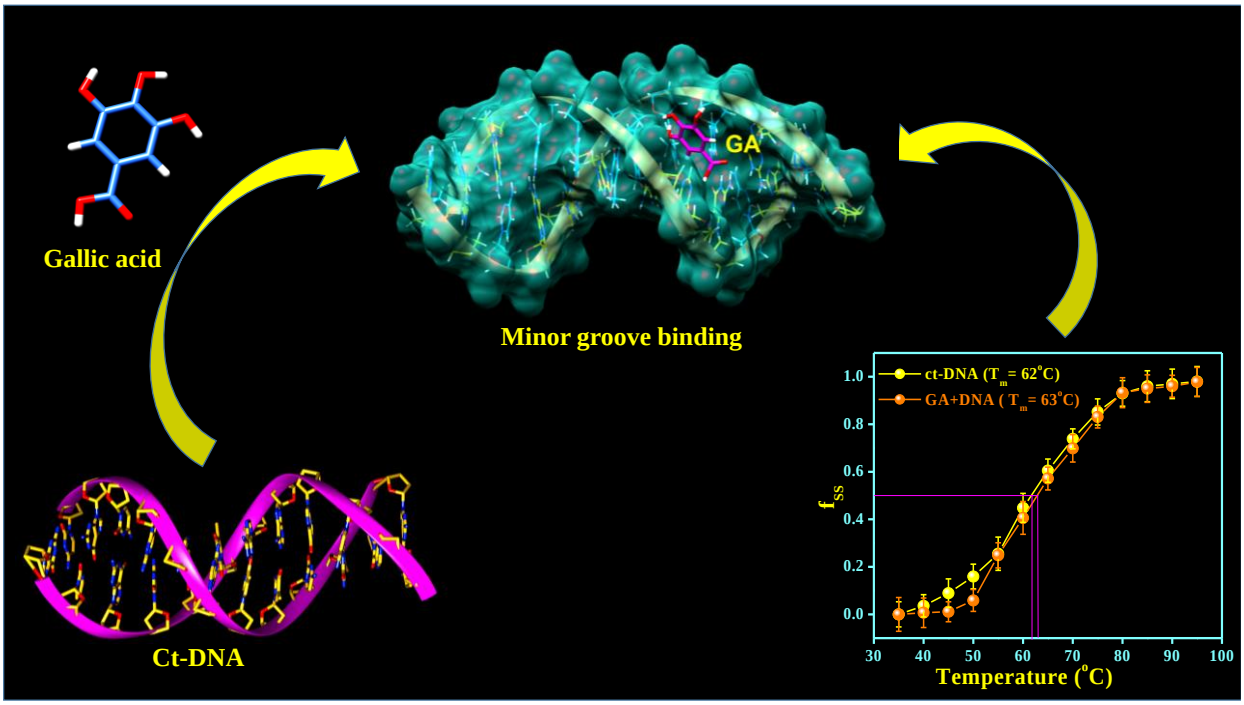

6.1. Introduction

The interaction of gallic acid (GA), a well-known polyphenol (sub-class: hydroxybenzoic acid), with DNA has been explored with the help of spectroscopic and theoretical methods. GA (Structure. 6.1) is predominantly present in green tea, different berries, mango, areca nut, wine, etc., and shows a wide variety of bioactivities such as antioxidant, anticancer, antimicrobial, anti-inflammatory etc. [Samuel et al., 2017; Abbasi et al., 2015; Albuquerque et al., 2021; Kahkeshani et al., 2019]. GA and its derivatives can prevent the oxidation and rancidity in oils and fats due to their free radical scavenging and antioxidant properties, and thus are recommended to be useful as food additives [Kahkeshani et al., 2019]. Previously, some works have compared the interaction of GA and other phenolic acids with DNA. Labieniec et.al. have reported that the binding affinity of GA with DNA is significantly less than other tested phenolic acids (tannic acid and ellagic acid) using fluorescence spectroscopic tool [Labieniec et al., 2006]. A better binding efficacy of GA compared to citric acid was reported by Chanphai et al. using UV-Vis experiments [Chanphai et al., 2022]. However, a detailed insight into the interaction of GA with DNA on molecular view is still rare. In the present work we have utilized spectroscopic methods such as fluorescence quenching, anisotropy measurements, DNA melting studies, circular dichroism, etc., to establish the interaction mechanism of GA-DNA system. Further, we have performed molecular docking studies to support our experimental findings. The current study on the interaction of GA with DNA is significant in terms of the potential applications of GA in different sectors. Besides, the significant observation acquired from these biophysical studies could be further extended to other phenolic acids to understand their molecular level mechanism.

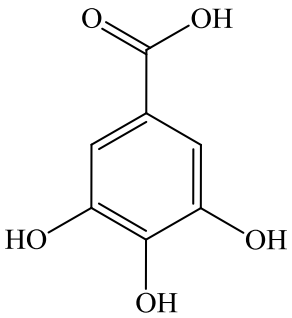

Structure 6.1. The chemical structure of GA

6.2. Materials and methods

6.2.1. Materials

Calf thymus DNA (ct-DNA), Ethidium bromide (EB) and potassium iodide (KI) were purchased from Sisco Research Laboratories (SRL, India) and used as received. Gallic acid (≥99.5%, powder) was purchased from Sigma-Aldrich, India and use after recrystallization in ethanol. Sodium chloride (NaCl) was purchased from Merck, India and used without further purification. Tris(hydroxymethyl)aminomethane (tris-HCl buffer) were purchased from Sigma-Aldrich, USA and 10 mM tris-HCl buffer of pH ~ 7.4 was prepared in triple distilled water. GA was dissolve in tris-HCl buffer. Stock solution of ct-DNA was prepared by dissolving the solid ct-DNA in 10 mM tris-HCl buffer and stored at 4 ºC for further use. The purity of ct-DNA was verified by monitoring the ratio of absorbance at 260 nm to that at 280 nm, which was in the range 1.8-1.9. The concentration of ct-DNA solution was determined by spectrophotometrically using molar absorption coefficient (ε_{260} = 6600 L mol^{-1} cm^{-1}) [Zhou et al., 2015]. Freshly prepared solutions were used for all the measurements.

6.2.2. Methods

6.2.2.1. Steady state fluorescence studies

To elucidate the binding interaction between GA and ct-DNA, steady state emission spectra and fluorescence anisotropy measurements were obtained with a Cary Eclipse fluorescence spectrophotometer (model G9800A) using 1.0 cm quartz cells. DNA does not show any endogenous fluorescence emission property and hence, the fluorescence emission of GA was monitored for the interaction between drug and DNA. The emission measurements of GA (25 µM) with varying concentrations of ct-DNA (0-100 µM) were made by exciting the samples at 260 nm. As the GA and ct-DNA show the same peak region in the UV-vis measurements, hence in the emission spectroscopy we have to correct the emission spectra to minimise the absorption contribution of ct-DNA. The fluorescence intensities were corrected for absorption of excited light and re-absorption of excitation light using the following equation [Lakowicz, 2006; Paul et al., 2017].

$$\mathbf{F_{corr} = F_{obs} \times antilog(\frac{OD_{ex}+OD_{em}}{2})} \qquad (6.1)$$

where, F_{corr} and F_{obs} are the corrected fluorescence intensity and observed background-subtracted fluorescence intensity of the sample under investigation, respectively; OD_{ex} and OD_{em} are the measured absorbance of the sample at the excitation and emission wavelengths, respectively [Lakowicz, 2006; Masum et al., 2014]. Emission and excitation studies were performed at room temperature. For fluorescence anisotropy measurements, the parallel and perpendicular emission polarizations were controlled using polarizer (cf. section 6.3.1.).

6.2.2.2. Circular Dichroism (CD) studies

CD measurements were performed on a JASCO J-815 spectrometer using a rectangular quartz cuvette of path length 1 cm at room temperature. The spectra were measured in the range of 220-350 nm. The CD profiles were taken an average of three successive scan with 20 nm per minute scan time and before measurements baseline was corrected appropriately. The response time was 4 s. During the experiments, the concentration of ct-DNA was fixed at 100 µM. The different sets of solutions with different ct-DNA to drug ratios (1:0, 1:0.5, 1:1) were prepared.

6.2.2.3. DNA melting studies

The DNA double helix melting temperature was determined using UV-Vis spectroscopy (Hitachi U-2910) by taking the absorbance at 260 nm in presence and absence of GA over a wide range of temperature from 35 °C to 90 °C. The sample contained ct-DNA (50 µM) alone and GA (50 µM)-ct-DNA (50 µM) complex in Tris-HCl buffer (pH 7.4 and 10 mM). The melting temperature (T_m) was determined by the following equation:

$$\mathbf{f_{ss} = \frac{A - A_0}{A_f - A_0}} \qquad (\mathbf{6.2})$$

where, f_{ss} corresponds to ct-DNA fraction as single strand, A_0 and A_f are the initial and final absorbance intensities respectively, A is the absorbance intensity corresponding to its temperature. The melting temperature (T_m) was determined from the midpoints of the curve based on f_{ss} versus temperature (T) plot [Silva et al., 2017].

6.2.2.4. Viscosity measurement studies

The viscosity measurements were performed with Ostwald viscometer immersed in the water bath at 30 °C and GA concentration was increased (0 µM, 5 µM, 10 µM, 15µM, 20 µM, 25 µM) with a fixed ct-DNA concentration (50 µM). The analysis was performed in triplicate and the flow time was measured using a digital stopwatch with an accuracy of ±0.2 second to evaluate the viscosity of free ct-DNA and GA-ct-DNA complex in a different molar ratio of GA to ct-DNA ([GA]/[ct-DNA]). The obtained data were presented as $(\eta/\eta_0)^{1/3}$ versus the ratio of [GA]/[ct-DNA], where η and η_0 are the viscosity of free ct-DNA and GA-ct-DNA complex respectively [Husain et al., 2017].

6.2.2.5. Potassium iodide (KI) quenching studies

Iodide quenching experiments were performed on the same fluorescence spectrophotometer as described above. The quenching study was performed in GA and GA-ct-DNA ([GA] = 20 µM; [ct-DNA] = 40 µM) complex solution by titrating with various concentration of KI (0-20 mM). The quenching constants (K_{SV}) for free and ct-DNA bound GA were calculated using Stern-Volmer equation [Lakowicz, 2006].

$$\frac{\mathbf{F_0}}{\mathbf{F}} = \mathbf{1} + \mathbf{K_{SV}[Q]} \qquad (\mathbf{6.3})$$

where, F_0 and F are the fluorescence intensities of free GA and ct-DNA-GA complex in the absence and presence of KI, respectively, and [Q] is the concentration of KI. K_{SV} is the Stern-Volmer quenching constant.

6.2.2.6. Competitive Displacement studies

A competitive displacement experiment was performed using a well-known intercalating probe ethidium bromide (EB). This experiment was carried out by adding a fixed amount of ct-DNA (75 µM) to EB (5 µM) solution and the mixture was titrated against the increasing concentration of GA (0-140 µM). The EB-ct-DNA complex was excited at 480 nm and the emission spectra were recorded in the region of 490 nm-800 nm [Mondal et al., 2021; Ramana et al., 2016].

6.2.2.7. Steady-state fluorescence anisotropy studies

Steady-state fluorescence anisotropy (r) measurements were performed on an Cary Eclipse fluorescence spectrophotometer (G9800A) equipped with a 1.0 cm path-length of rectangular quartz cell and a pair of polariser was used with excitation and emission wavelengths set to 257 nm and 353 nm respectively. The excitation and emission bandwidths were set as 10 nm and 5 nm respectively. The r was then calculated by the following equations [Banerjee et al., 2012]:

$$\mathbf{r} = (\mathbf{I_{VV}} - \mathbf{G} \times \mathbf{I_{VH}})/(\mathbf{I_{VV}} + \mathbf{2G} \times \mathbf{I_{VH}}) \qquad (\mathbf{6.4})$$

$$\mathbf{G} = \frac{\mathbf{I_{HV}}}{\mathbf{I_{HH}}} \qquad (\mathbf{6.5})$$

where, I is the fluorescence emission intensity and the suffix VV denotes both the excitation and emission polarizers to be vertically aligned and VH indicates a vertically aligned excitation polarizer and horizontally aligned emission polarizer, HV corresponds to horizontally polarized excitation and vertically polarized excitation and so on. G is the correction factor. Titrations were carried out by various concentration of ct-DNA ranging from 0-100 μM with a fixed concentration of GA (30 μM) solution.

6.2.2.8. Molecular Docking Studies

To understand the site of binding when GA interacts with ct-DNA, molecular docking study was carried out. The three-dimensional structure of GA was prepared and optimized in Avogadro software [Hanwell et al., 2012] in order to obtain the lowest energy structure of the ligand. The DNA structure was downloaded from RCSB [Neidle et al., 1999] (PDB ID: 453D) and the docking study was carried out using AutoDock Vina [Trott et al., 2010] after removing the ligands from the PDB file. The grid size used in this case was 20×22×42 Å with centre at x = 15.115; y = 20.786; z = 8.718. Out of multiple docked structures, the GA-ct-DNA bound structure with the lowest energy (highest negative ΔG value) was selected for the study. Analysis of neighboring DNA base pairs, H-bonding calculation and RMSD calculation were carried out using UCSF Chimera software [Pettersen et al., 2004].

6.3. Results and discussions

6.3.1. Analysis of steady state fluorescence studies

Due to the similarity of the absorbance region of GA (λ_{max} = 255 nm, inset of Fig. 6.1) and DNA (λ_{max} = 260 nm) [Mondal et al., 2021], the UV-Vis titration experiment washampered (data not shown). Thus, we resorted to only fluorescence titration experiment with GA and DNA. As already mentioned in Section 6.2.2.1, the possibility of re-absorption and inner filter effect was removed by applying Equation 6.1. Gradual addition of ct-DNA enhanced the fluorescence intensity of GA. Thus, an indication of some sort of complexation and structural change of GA in ct-DNA environment (vide Fig. 6.1) was evident. The observation was further supported by theoretical studies.

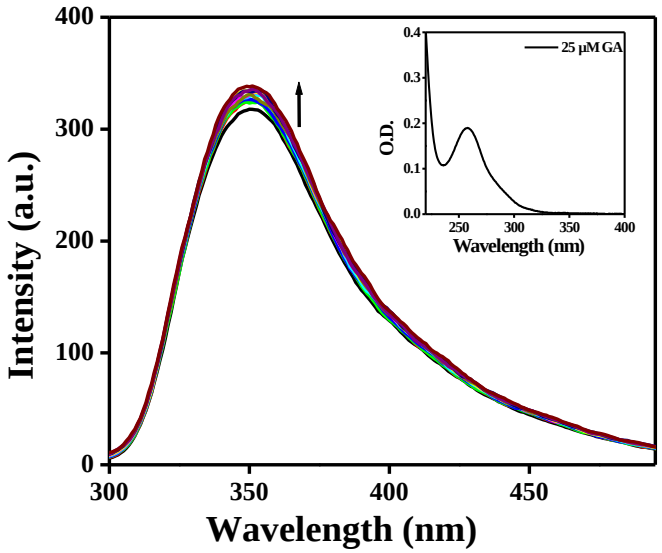

Figure 6.1. Fluorescence titration spectra of GA (25 μM) with various concentration of ct-DNA (0-100 μM). (inset: absorption spectra of free gallic acid)

6.3.2. Iodide quenching study

Fluorescence quenching of small molecules by KI is a well-established method to primary characterize the binding type of small molecules to DNA. In brief, intercalating molecules are well protected into DNA base pairs and thus, its fluorescence is less quenched by KI. Whereas, groove/electrostatic binders are almost in an open position and thus, its fluorescence is well affected by KI [Mondal et al., 2021]. Thus, the amount of quenching by KI is comparable for both free molecule and DNA bound molecule, indicating the groove binding. In this view, the fluorescence quenching studies of GA were performed in the absence and presence of ct-DNA taking KI as quencher molecule and the results were quantified via Stern-Volmer equation [Lakowicz, 2006]. As can be evident from Fig. 6.2, K_{SV} of the DNA bound GA (20 µM) was almost similar to that of free GA (20 µM). However, the investigating molecule, i.e., GA, is a negatively charged molecule and the nucleic acids are also highly negatively charged hence, the occurrence of electrostatic interaction can be ruled out. Thus, the experimental observations unambiguously established that the mode of binding of GA to ct-DNA is groove binding.

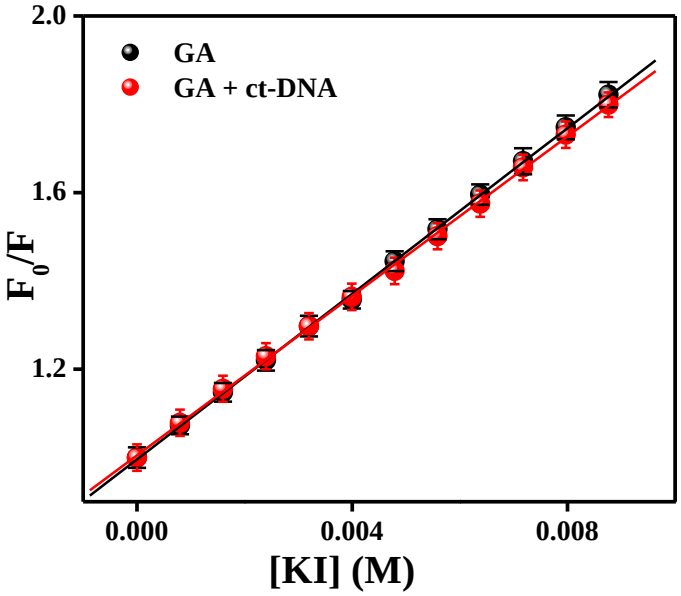

Figure 6.2. Stern-Volmer quenching plot of GA (20 µM) by varying KI (0-0.009 M) concentration in the absence and presence of ct-DNA

6.3.3. Viscosity measurements

Viscosity measurement is an authenticate technique for the evaluation of mode of binding between small molecule to ct-DNA [Mati et al., 2013]. When a classical intercalating ligand binds to ct-DNA, the nitrogen base pair of ct-DNA are separated to accommodate the intercalating ligand that leads to lengthening of the DNA helix, and hence, the viscosity of ct-DNA increases. However, for groove binding, insignificant changes in the viscosity of ct-DNA are generally noticed. Hence, we have plotted relative specific viscosity $(\eta/\eta_0)^{1/3}$ versus the [GA]/[ct-DNA] in Fig. 6.3. The result illustrated an insignificant variation in the relative specific viscosity of ct-DNA in the presence of GA. Thus, groove binding mechanism was substantiated by the experiment.

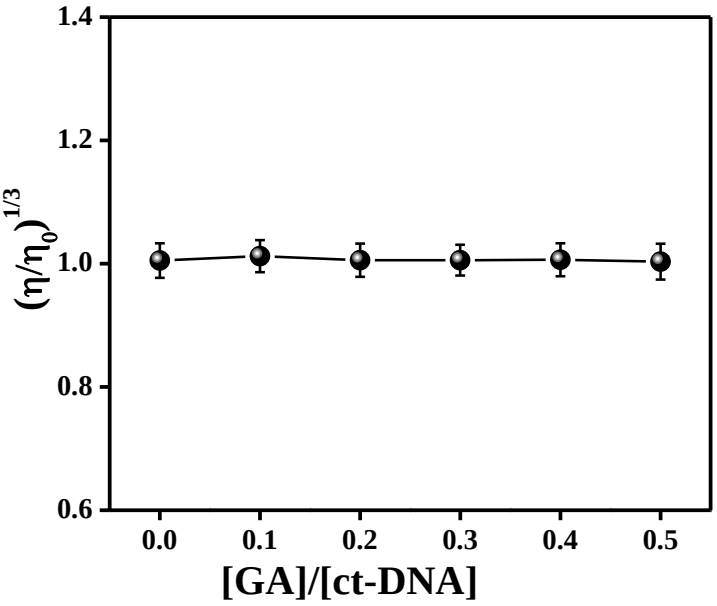

Figure 6.3. Viscosity measurement plot of ct-DNA (50 μM) with increasing concentration of GA

6.3.4. Circular dichroism (CD) experiments

The far-UV CD spectra of DNA duplex in aqueous buffer display two bands, viz., positive band (~273-280 nm for a canonical B-form) and negative band (~245 nm, due to right handed helicity) [Bhowmik et al., Manna et al., 2012]. To determine the GA induced changes in the secondary structure of DNA, the intrinsic far-UV CD spectra of DNA was monitored in presence of increasing concentration of GA (Fig. 6.4). It is well-established in literature that both positive and negative bands of DNA duplex perturb remarkably during intercalative binding mode with small molecules. In contrast, the base stacking and helicity bands of DNA are not perturbed for groove binding [Yang et al., 2017; Manojkumar et al., 2015]. In our case, addition of GA had an insignificant effect on the CD spectrum of ct-DNA which again supported the occurrence of groove binding mode in the interaction of GA with ct-DNA.

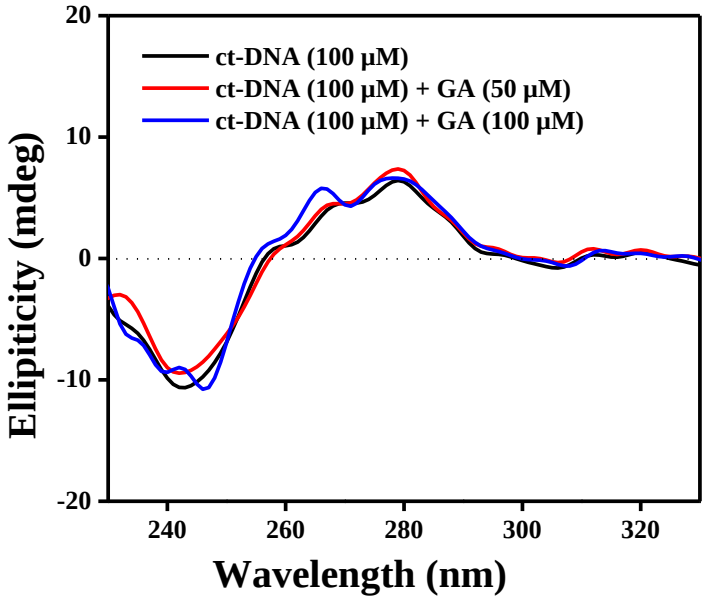

Figure 6.4. Far-UV CD spectra of ct-DNA on the addition of varying concentration of GA

6.3.5. Competitive displacement experiment

To further verify the mode of binding, competition binding assay experiments were performed using the well-established DNA intercalator molecule Ethidium bromide (EB). EB is a well-known dye that binds strongly to the intercalative site of double standard DNA, producing a

bright and intense fluorescence. Displacement of EB by a competing ligand will cause in the decrease of fluorescence intensity of DNA-EB complex which directly indicates about the intercalating nature of the competing ligand [Song et al., 2000; Lyles et al., 2002; Ramana et al., 2016]. In the present study, GA was unable to decrease the fluorescence intensity of DNA-EB complex (vide Fig. 6.5) which again supported our previous findings of groove binding mode.

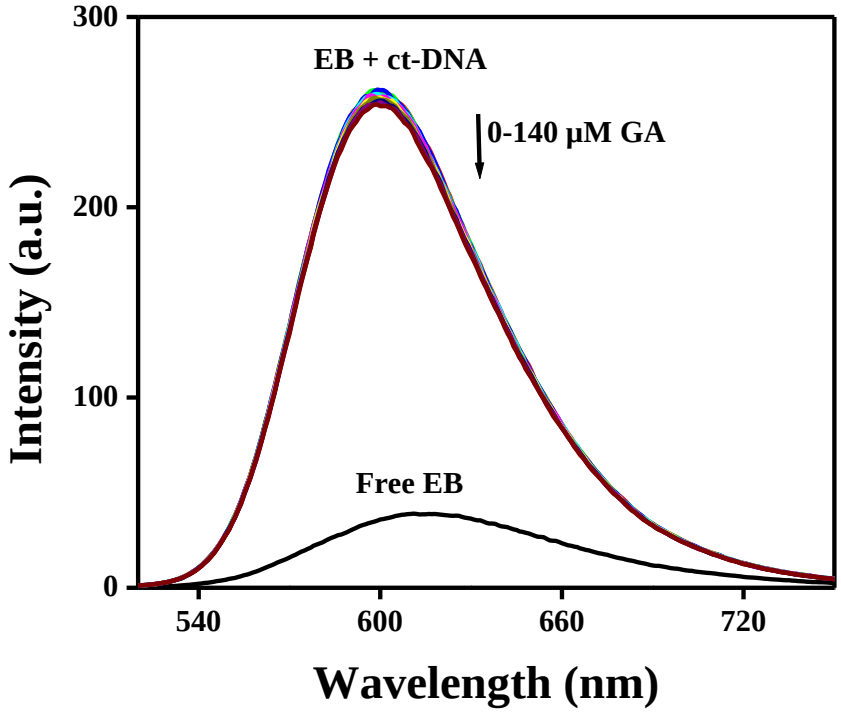

Figure 6.5. Fluorescence emission spectra of native EB and EB-ct-DNA complex with increasing concentration of GA (0-140 µM)

6.3.6. DNA melting studies

The double-helical structure of DNA is mainly stabilized due to hydrogen bonds between purines and pyrimidines of opposite strand and the base stacking interactions. With increasing temperature, the above forces are weakened resulting in the double-helical structure of DNA to dissociate into single strands [Wijeratne et al., 2012; Mergny et al., 1992; Nagababu et al., 2009].

Intercalation of small molecules within the double helix leads to enhancement of the DNA thermal stability by about 5-8 °C due to stabilizing of π-π stacking interactions. Whereas, for

non-intercalative binding, i.e., groove binding, a little or no significant change is observed in melting temperature (T_m) [Yasmeen et al., 2017]. The values of T_m for ct-DNA and GA-ct-DNA complex were obtained from Fig. 6.6 and the values were 62 °C and 63 °C respectively. The small change (1°C) in melting temperature indicated the occurance of groove binding between ct-DNA and GA.

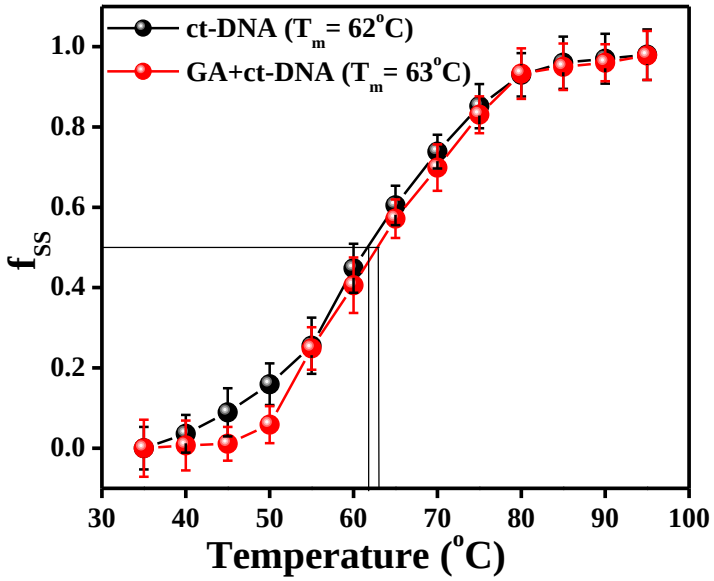

Figure 6.6. Thermal melting curve of free ct-DNA and GA-ct-DNA complex at pH 7.4

6.3.7. Fluorescence anisotropy

When small molecules intercalates with the DNA helix, the rotational motion of the small molecule get restricted. This is due to the insertion of small molecules into the DNA double helix. Hence fluorescence anisotropy increases significantly for intercalative type binding, but for groove binding the fluorescence anisotropy of the small molecule almost remains the same [Das et al., 2007; Wang et al., 2018]. Our observation indicated that the flexibility of GA was little changed with increasing ct-DNA concentration into GA (30 µM) solution (vide Fig. 6.7). Hence the interaction between GA with ct-DNA was further confirmed to be groove binging.

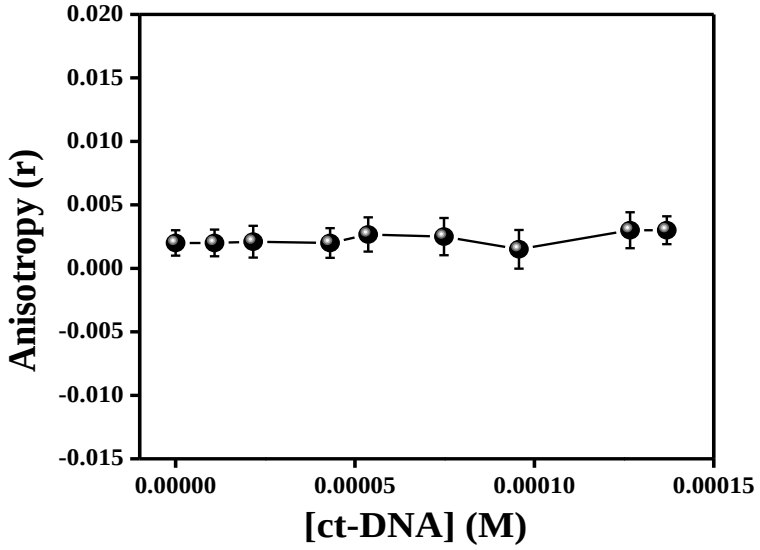

Figure 6.7. Fluorescence anisotropy plot of GA (30 µM) and ct-DNA (0-100 µM)

6.3.8. Molecular Docking Study

Docking studies with DNA and GA exhibited groove binding with a binding affinity value of -5.4 kcal/mol. Upon further investigation into the docked structure, it can be found that GA interacts with DNA bases through hydrogen bonding interaction.

GA is a polyphenolic compound which exists as a planar structure (vide Structure 6.1). Due to its planarity it is expected to intercalate into the stacked nucleotide base pairs. However, the docked structure (Fig. 6.8) showed GA to exhibit groove binding (minor groove) with B-DNA without showing any intercalation. This can be explained on the basis of changes in the conformational GA structure upon binding to DNA. Comparing the structure of GA before and after binding to DNA (Fig. 6.8. (A), (B), (C)), it can be seen that the ligand undergoes appreciable conformational changes which is reflected from its RMSD value of 3.17 Å (yellow: native GA, Blue: docked GA, vide Fig. 6.8. (C)). Such conformational changes occur due to the rotation of the -OH and COOH bond in GA. Although this does not permit the entry of the ligand into the stacked nucleotide base pairs, but it allows the molecule to lay down on one of the grooves [Di Pietro et al., 2021]. In addition, GA is negatively charged which can prevent its close association with DNA, which is itself a negatively charged species, thereby preventing intercalation. The

groove binding of GA is facilitated through the multiple hydrogen bonding with the base pairs (Table 6.1). The COOH groups can associate with two hydrogen bonds whereas one of the phenolic -OH groups can also form hydrogen bond with the nucleotide bases near it. This leads to the stabilization of the DNA-GA complex as seen from the appreciable binding affinity from experimental studies. Small increment in the fluorescence intensity of GA is mainly due to the enhanced binding and may be also due to the change in its planar structure (vide Section 6.3.1, Fig. 6.1)

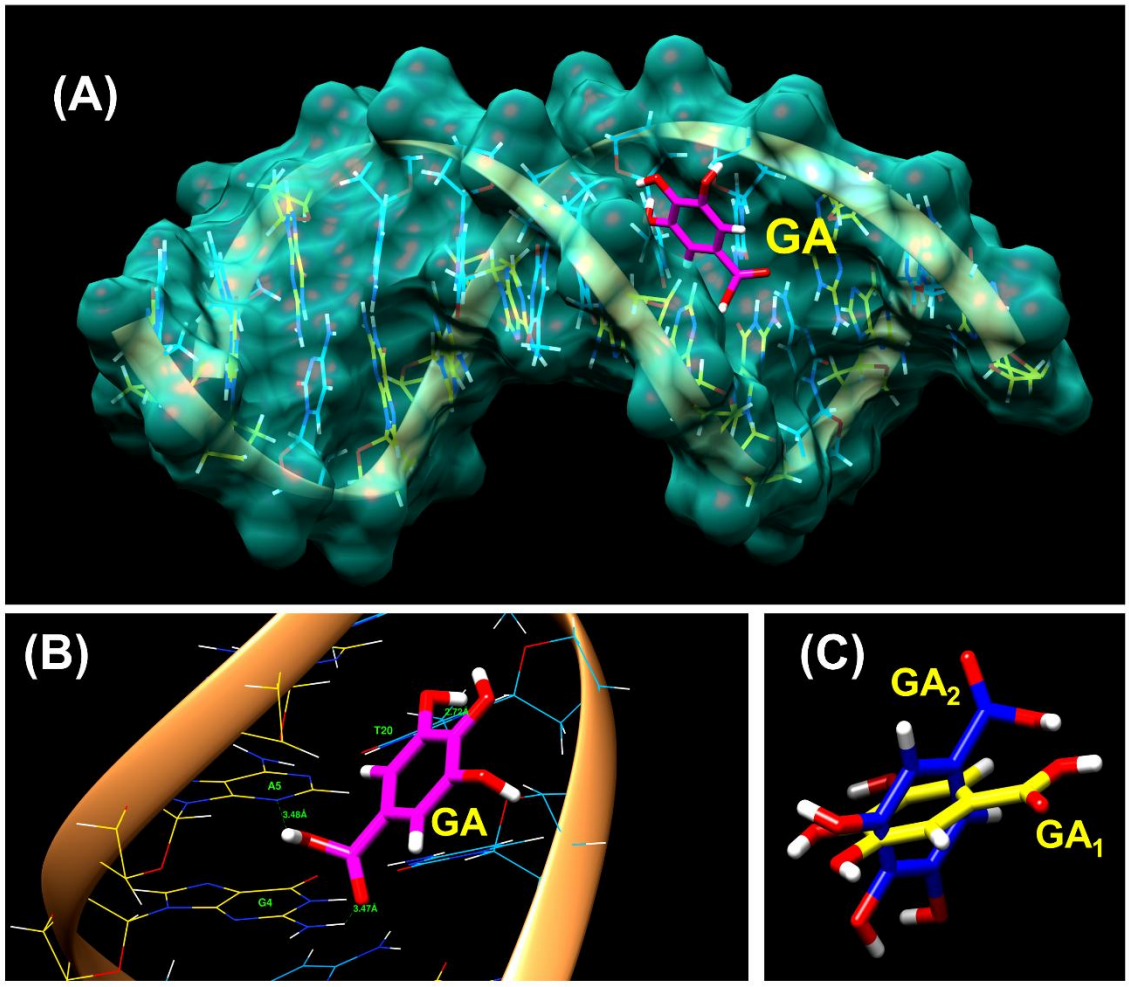

Figure 6.8. Molecular docking of GA with DNA: (A) GA binds at the groove of DNA as seen from the docked structure; (B) Possible hydrogen bonding between GA and base pairs of DNA; (C) Two different conformations of GA are shown superimposed over one another (GA1 shown in yellow: before docking and GA1 shown in blue: after docking) with RMSD value of 3.17 Å

Table 6.1. Hydrogen bnding distance between GA and nearby DNA bases pairs

DNA residue	GA atom	Distance (in Å)
Adenine (A5-N)	OH (of COOH)	3.48
Guanine (G4-NH_2)	C=O (of COOH)	3.47
Thamine (T20-C=O)	O-H (meta hydroxyl group)	2.72

6.4. Conclusion

In conclusion, we have investegated the binding mechanism of GA with ct-DNA via different biophysical techniques. GA was found to interact with ct-DNA through groove binding mode. The groove binding mode was confirmed from all the experimental observations. Molecular docking studies also suggested the involvement of groove binding between GA and ct-DNA with a favorable binding energy of -5.4 kcal/mol. Hydrogen bonding as well as van der Waal's forces played a significant role in the binding of GA to ct-DNA.

6.5. References

Abbasi, A.M., Guo, X., Fu, X., Zhou, L., Chen, Y., Zhu, Y., Yan, H., Liu, R.H., 2015. Comparative assessment of phenolic content and in vitro antioxidant capacity in the pulp and peel of mango cultivars. International Journal of Molecular Sciences, 16, 13507-13527.

Albuquerque, B.R., Heleno, S.A., Oliveira, M.B.P., Barros, L., Ferreira, I.C., 2021. Phenolic compounds: Current industrial applications, limitations and future challenges. Food & Function. 12, 14-29.

Banerjee, M., Pal, U., Subudhhi, A., Chakrabarti, A., Basu, S., 2012. Interaction of Merocyanine 540 with serum albumins: photophysical and binding studies. Journal of Photochemistry and Photobiology B: Biology. 108, 23-33.

Bhowmik, D., Hossain, M., Buzzetti, F., D'Auria, R., Lombardi, P., Kumar, G.S., 2012. Biophysical studies on the effect of the 13 position substitution of the anticancer alkaloid berberine on its DNA binding. The Journal of Physical Chemistry B. 116, 2314-2324.

Chanphai, P., Tajmir-Riahi, H.A., 2022. DNA acidification by citric acid and gallic acid: acid binding site and DNA structural dynamics. Journal of Biomolecular Structure and Dynamics. 40, 2389-2394.

Das, P., Chakrabarty, A., Haldar, B., Mallick, A., Chattopadhyay, N., 2007. Effect of cyclodextrin nanocavity confinement on the photophysics of a β-carboline analogue: a spectroscopic study. The Journal of Physical Chemistry B. 111, 7401-7408.

Di Pietro, M.L., La Ganga, G., Nastasi, F., Puntoriero, F., 2021. Ru (II)-Dppz Derivatives and Their Interactions with DNA: Thirty Years and Counting. Applied Sciences. 11, 3038.

Hanwell, M.D., Curtis, D.E., Lonie, D.C., Vandermeersch, T., Zurek, E., Hutchison, G.R., 2012. Avogadro: an advanced semantic chemical editor, visualization, and analysis platform. Journal of Cheminformatics. 4, 1-17.

Husain, M.A., Ishqi, H.M., Sarwar, T., Rehman, S.U., Tabish, M., 2017. Interaction of indomethacin with calf thymus DNA: a multi-spectroscopic, thermodynamic and molecular modelling approach. Med Chem Comm. 8, 1283-1296.

Kahkeshani, N., Farzaei, F., Fotouhi, M., Alavi, S.S., Bahramsoltani, R., Naseri, R., Momtaz, S., Abbasabadi, Z., Rahimi, R., Farzaei, M.H., Bishayee, A., 2019. Pharmacological effects of gallic acid in health and diseases: A mechanistic review. Iranian Journal of Basic Medical Sciences. 22, 225-237.

Labieniec, M., Gabryelak, T., 2006. Interactions of tannic acid and its derivatives (ellagic and gallic acid) with calf thymus DNA and bovine serum albumin using spectroscopic method. Journal of Photochemistry and Photobiology B: Biology. 82, 72-78.

Lakowicz, J.R. ed., 2006. Principles of fluorescence spectroscopy. Boston, MA: springer US.

Lyles, M.B., Cameron, I.L., 2002. Interactions of the DNA intercalator acridine orange, with itself, with caffeine, and with double stranded DNA. Biophysical Chemistry. 96, 53-76.

Manna, A., Chakravorti, S., 2012. Modification of a styryl dye binding mode with calf thymus DNA in vesicular medium: from minor groove to intercalative. The Journal of Physical Chemistry B. 116, 5226-5233.

Manojkumar, K., Prabhu Charan, K.T., Sivaramakrishna, A., Jha, P.C., Khedkar, V.M., Siva, R., Jayaraman, G., Vijayakrishna, K., 2015. Biophysical characterization and molecular docking studies of imidazolium based polyelectrolytes-DNA complexes: Role of hydrophobicity. Biomacromolecules. 16, 894-903.

Masum, A.A., Chakraborty, M., Pandya, P., Halder, U.C., Islam, M.M., Mukhopadhyay, S., 2014. Thermodynamic study of rhodamine 123-calf thymus DNA interaction: determination of calorimetric enthalpy by optical melting study. The Journal of Physical Chemistry B. 118, 13151-13161.

Mati, S.S., Roy, S.S., Chall, S., Bhattacharya, S., Bhattacharya, S.C., 2013. Unveiling the groove binding mechanism of a biocompatible naphthalimide-based organoselenocyanate with calf thymus DNA: an “ex vivo” fluorescence imaging application appended by biophysical experiments and molecular docking simulations. The Journal of Physical Chemistry B. 117, 14655-14665.

Mergny, J.L., Duval-Valentin, G., Nguyen, C.H., Perrouault, L., Faucon, B., Rougee, M., Montenay-Garestier, T., Bisagni, E., Helene, C., 1992. Triple helix-specific ligands. Science. 256, 1681-1684.

Mondal, P., Sengupta, P., Pal, U., Saha, S., Bose, A., 2021. Biophysical and theoretical studies of the interaction between a bioactive compound 3, 5-dimethoxy-4-hydroxycinnamic acid with calf thymus DNA. Spectrochimica Acta Part A: Molecular and Biomolecular Spectroscopy. 245, 118936-118950.

Nagababu, P., Latha, J.N.L., Prashanthi, Y., Satyanarayana, S., 2009. DNA-Binding and Photocleavage Studies of Cobalt (III) Ethylenediamine Complexes: $[Co\ (en)_2phen]^{3+}$ and $[Co\ (en)_2bpy]^{3+}$, Journal of Chemical and Pharmaceutical Research. 1, 238-249.

Neidle, S., Rayner, E.L., Simpson, I.J., Smith, N.J., Mann, J., Baron, A., Opoku-Boahen, Y., Fox, K.R., Hartley, J.A., Kelland, L.R., 1999. Symmetric bis-benzimidazoles: new sequence-selective DNA-binding molecules. Chemical Communications. 10, 929-930.

Paul, S., Sepay, N., Sarkar, S., Roy, P., Dasgupta, S., Sardar, P.S., Majhi, A., 2017. Interaction of serum albumins with fluorescent ligand 4-azido coumarin: spectroscopic analysis and molecular docking studies. New Journal of Chemistry. 41, 15392-15404.

Pettersen, E.F., Goddard, T.D., Huang, C.C., Couch, G.S., Greenblatt, D.M., Meng, E.C., Ferrin, T.E., 2004. UCSF Chimera-a visualization system for exploratory research and analysis. Journal of Computational Chemistry. 25, 1605-1612.

Ramana, M.M.V., Betkar, R., Nimkar, A., Ranade, P., Mundhe, B., Pardeshi, S., 2016. Synthesis of a novel 4H-pyran analog as minor groove binder to DNA using ethidium bromide as fluorescence probe. Spectrochimica Acta Part A: Molecular and Biomolecular Spectroscopy. 152, 165-171.

Samuel, K.G., Wang, J., Yue, H.Y., Wu, S.G., Zhang, H.J., Duan, Z.Y., Qi, G.H., 2017. Effects of dietary gallic acid supplementation on performance, antioxidant status, and jejunum intestinal morphology in broiler chicks. Poultry Science. 96, 2768-2775.

Silva, M.M., Nascimento, E.O., Júnior, E.F.S., de Araujo Junior, J.X., Santana, C.C., Grillo, L.A.M., de Oliveira, R.S., Costa, P.R., Buarque, C.D., Santos, J.C.C., Figueiredo, I.M., 2017. Interaction between bioactive compound 11a-N-tosyl-5-deoxi-pterocarpan (LQB-223) and Calf thymus DNA: Spectroscopic approach, electrophoresis and theoretical studies. International Journal of Biological Macromolecules. 96, 223-233.

Song, Y., Kang, J., Zhou, J., Wang, Z., Lu, X., Wang, L., Gao, J., 2000. Study on the fluorescence spectra and electrochemical behavior of ZnL2 and Morin with DNA. Spectrochimica Acta Part A: Molecular and Biomolecular Spectroscopy. 56, 2491-2497.

Trott, O., Olson, A.J., 2010. AutoDock Vina: improving the speed and accuracy of docking with a new scoring function, efficient optimization, and multithreading. Journal of Computational Chemistry. 31, 455-461.

Wang, X. and Cui, F., 2018. Binding characteristics of imidazolium-based ionic liquids with calf thymus DNA: Spectroscopy studies. Journal of Fluorine Chemistry, 213, 68-73.

Wijeratne, S.S., Patel, J.M., Kiang, C.H., 2012. Melting transitions of DNA-capped gold nanoparticle assemblies. In Reviews in Plasmonics, Springer, New York. 2010, 269-282.

Yang, H., Tang, P., Tang, B., Huang, Y., He, J., Li, S., Li, H., 2017. Studies of DNA-binding properties of lafutidine as adjuvant anticancer agent to calf thymus DNA using multi-spectroscopic approaches, NMR relaxation data, molecular docking and dynamical simulation. International Journal of Biological Macromolecules. 99, 79-87.

Yang, H., Tang, P., Tang, B., Huang, Y., Xiong, X., Li, H., 2017. Novel poly (ADP-ribose) polymerase inhibitor veliparib: biophysical studies on its binding to calf thymus DNA. RSC Advances. 7, 10242-10251.

Yasmeen, S., Qais, F.A., 2017. Unraveling the thermodynamics, binding mechanism and conformational changes of HSA with chromolyn sodium: Multispecroscopy, isothermal titration calorimetry and molecular docking studies. International Journal of Biological Macromolecules. 105, 92-102.

Zhou, X., Zhang, G., Pan, J., 2015. Groove binding interaction between daphnetin and calf thymus DNA. International Journal of Biological Macromolecules. 74, 185-194.